Available online at www.sciencedirect.com
ScienceDirect
International Journal of Heat and Mass Transfer 51 (2008) 4327–4341
International Journal of HEAT and MASS TRANSFER
www.elsevier.com/locate/ijhmt

Fluid flow and heat transfer characteristics of low temperature two-phase micro-channel heat sinks – Part 2. Subcooled boiling pressure drop and heat transfer

Jaeseon Lee, Issam Mudawar *

Boiling and Two-Phase Flow Laboratory (BTPFL), Purdue University International Electronic Cooling Alliance (PUIECA), Mechanical Engineering Building, 585 Purdue Mall, West Lafayette, IN 47907-2088, USA

Received 13 June 2007; received in revised form 16 February 2008
Available online 22 May 2008

Abstract

This second part of a two-part study explores the performance of a new cooling scheme in which the primary working fluid flowing through a micro-channel heat sink is indirectly cooled by a refrigeration cooling system. The objective of this part of study is to explore the pressure drop and heat transfer characteristics of the heat sink. During single-phase cooling, pressure drop decreased with increasing heat flux because of decreased liquid viscosity. However, pressure drop began increasing with increasing heat flux following bubble departure. These opposite trends produced a minimum in the variation of pressure drop with heat flux. Increasing liquid subcooling decreased two-phase pressure drop because of decreased void fraction caused by strong condensation at bubble interfaces as well as decreased likelihood of bubble coalescence. It is shown macro-channel subcooled boiling pressure drop and heat transfer correlations are unsuitable for micro-channel flows. However, two new modified correlations produced good predictions of the present heat transfer data.

1. Introduction

1.1. Application of subcooled flow boiling for high-flux cooling

Flow boiling is known for its ability to produce very high convective heat transfer coefficients, which is why it is widely used in many applications demanding high-flux heat removal. Two main regimes are possible with flow boiling, subcooled and saturated; each is also made up of sub-regimes. Subcooled and saturated boiling can occur concurrently in a long heated channel if the incoming fluid is supplied below saturation temperature corresponding to the inlet pressure. With an inlet thermodynamic equilibrium quality below zero, subcooled boiling prevails in the inlet region and, as the quality rises along the channel, a point is reached where transition to saturated boiling takes effect. Because of large differences in void fraction, the heat transfer mechanism for subcooled boiling is categorically different from that for saturated boiling. In the subcooled region, liquid flow is more abundant and phase-change occurs mostly by bubble formation at the wall. High void fractions in saturated boiling are associated with churn, slug and annular flows in which bubble nucleation is gradually replaced by evaporation of a residual liquid film at the heated wall.

In general, higher average heat transfer coefficients are possible with subcooled flow boiling than with saturated. Critical heat flux (CHF) is also greater for subcooled boiling. Furthermore, there are drastic differences in CHF mechanism between the two regimes. Subcooled CHF (commonly referred to as "departure from nucleate boiling" or DNB for short) is the result of localized vapor blanket formation along the heated wall even while liquid is abundant in the core. On the other hand, CHF in saturated boiling occurs in a predominantly liquid deficient region and is usually the result of dryout of the annular liquid film.

* Corresponding author. Tel.: +1 (765) 494 5705; fax: +1 (765) 494 0539.
E-mail address: mudawar@ecn.purdue.edu (I. Mudawar).

0017-9310/$ - see front matter © 2008 Elsevier Ltd. All rights reserved.
doi:10.1016/j.ijheatmasstransfer.2008.02.013

Nomenclature

A_{base}	total base area of micro-channel heat sink
Bo	Boiling number
CHF	critical heat flux
c_p	specific heat
D_h	hydraulic diameter of micro-channel
f	friction factor
F_f	constant in Eqs. (10) and (11)
G	mass velocity
h	heat transfer coefficient; enthalpy
$\bar{h}$	mean heat transfer coefficient across base of heat sink
H_{ch}	height of micro-channel
h_{fg}	latent heat of vaporization
Ja^*	modified Jacob number
L	length of micro-channel
$\dot{m}$	total mass flow rate of coolant entering heat sink
N	constant in Eq. (5)
Nu	Nusselt number
ONB	onset of nucleate boiling
P	pressure
ΔP	pressure drop
Pr	Prandtl number
q''	heat flux through heat sink base area
Re_{Dh}	Reynolds number based on hydraulic diameter of micro-channel
T	temperature
TS	test section
T_w	base wall temperature of micro-channel heat sink
$\overline{T}_w$	mean base wall temperature of micro-channel heat sink
v	specific volume
W_{ch}	width of micro-channel
W_w	half-width of solid wall separating micro-channels
We^*	modified Weber number
x_e	thermodynamic equilibrium quality
z	streamwise coordinate

Greek symbols

β	channel aspect ratio
ϕ	fluid phase indication
μ	viscosity
ρ	density
σ	surface tension

Subscripts

–	phase averaged property
1, 2, 3	measurement locations
A	accelerational pressure drop component
ad	adiabatic
bd	bubble departure from wall
ch	micro-channel
e	thermodynamic equilibrium
exp	experimental (measured)
F	frictional pressure drop component
f	liquid
g	saturated vapor
in	micro-channel inlet
ONB	onset of nucleate boiling
out	micro-channel outlet
pred	predicted
sat	saturated
sc	subcooled
sp	single-phase
sub	subcooling
tp	two-phase

Clearly, subcooled boiling is quite advantageous for high-flux applications. This regime can be achieved in a variety of ways, the two most common are increasing mass velocity and increasing liquid subcooling at the inlet. Channel geometry can also have a strong effect on the extent of the subcooled boiling region. For example, channels with small length-to-diameter ratio are more likely to maintain subcooled boiling.

As discussed in Part 1 of this study [1], recent advances in microelectronics have triggered unprecedented increases in heat dissipation. This trend has spurred the development of many types of phase-change cooling schemes that are aimed at both removing the heat and maintaining low surface temperatures. Micro-channel heat sinks have emerged as one of the most effective thermal solutions, given their compactness and ability to produce very high heat transfer coefficients while demanding low coolant flow rates and small coolant inventory.

Early micro-channel studies were focused mainly on single-phase flow. An often-cited study by Tuckerman and Pease [2] proved such devices could dissipate up to 790 W/cm^2 from a simulated electronic heat source using water as working fluid. Interestingly, flow boiling in micro-channels has been the subject of intense study since the mid-1970s at the Massachusetts Institute of Technology Energy Laboratory for cooling of electrodes in magnetohydrodynamic energy converters and turbine blades [3]. A fairly large number of studies of flow boiling in micro-channels have been published since the mid-1990s, e.g., [4–16]. Mudawar and Bowers [7] showed highly subcooled and high mass velocity flow boiling of water in small diameter tubes could safely dissipate heat fluxes as high as 27,000 W/cm^2.

What have been lacking so far are thermal solutions for defense electronics that are anticipated to reach and exceed 1000 W/cm^2 in the near future, and which must be main-

tained at relatively low temperatures (below 125 °C) using inert dielectric coolants [17]. Such coolants possess very poor thermal transport properties, making the attainment of this cooling performance quite elusive.

As discussed in part 1 of this study, the present authors have developed an indirect refrigeration cooling scheme where the primary coolant flowing through the micro-channel heat sink is brought to a very low temperature at the micro-channel inlet in order to maintain highly subcooled conditions. Despite the small hydraulic diameter of the micro-channels, the low coolant temperature was shown to preserve subcooled boiling along much of the micro-channel length, especially at high mass velocities.

The primary objectives of this part of the study are to (1) explore the parametric trends of subcooled boiling pressure drop and heat transfer, (2) evaluate the effectiveness of previous correlations in predicting the new data, and (3) develop more accurate correlations for both pressure drop and heat transfer.

1.2. Thermodynamic considerations in subcooled flow boiling

As indicated in the previous section, subcooled flow boiling occurs when liquid is supplied into a heated channel is subcooled state. Single-phase heat transfer to liquid occurs over a finite length of the channel until bubbles begin to form along the wall, indicating transition to subcooled boiling. As core liquid temperature continues to rise along the channel, transition to saturated boiling ultimately ensues. Because of strong departure from thermodynamic equilibrium, predicting subcooled boiling is a very challenging endeavor, especially in the ability to develop reliable models for pressure drop and heat transfer.

Fig. 1 shows a simplified schematic of the transitions from single-phase cooling to saturated boiling. Following a classification by Collier and Thome [18], the subcooled boiling region is comprised of two zones. The first is a *highly subcooled zone* whose upstream edge corresponds to the onset of boiling, z_{ONB}. Within this zone, bubbles are able to form but show minor growth while still attached to the wall. Suppressed bubble growth in this zone is the result of a thermal balance between superheat effects at the wall and condensation along the bubble interface. A second *developed subcooled zone* begins at z_{bd} at which bubbles begin to detach into the liquid flow where they condense slightly but are able to endure and even coalesce with one another. The second zone extends downstream

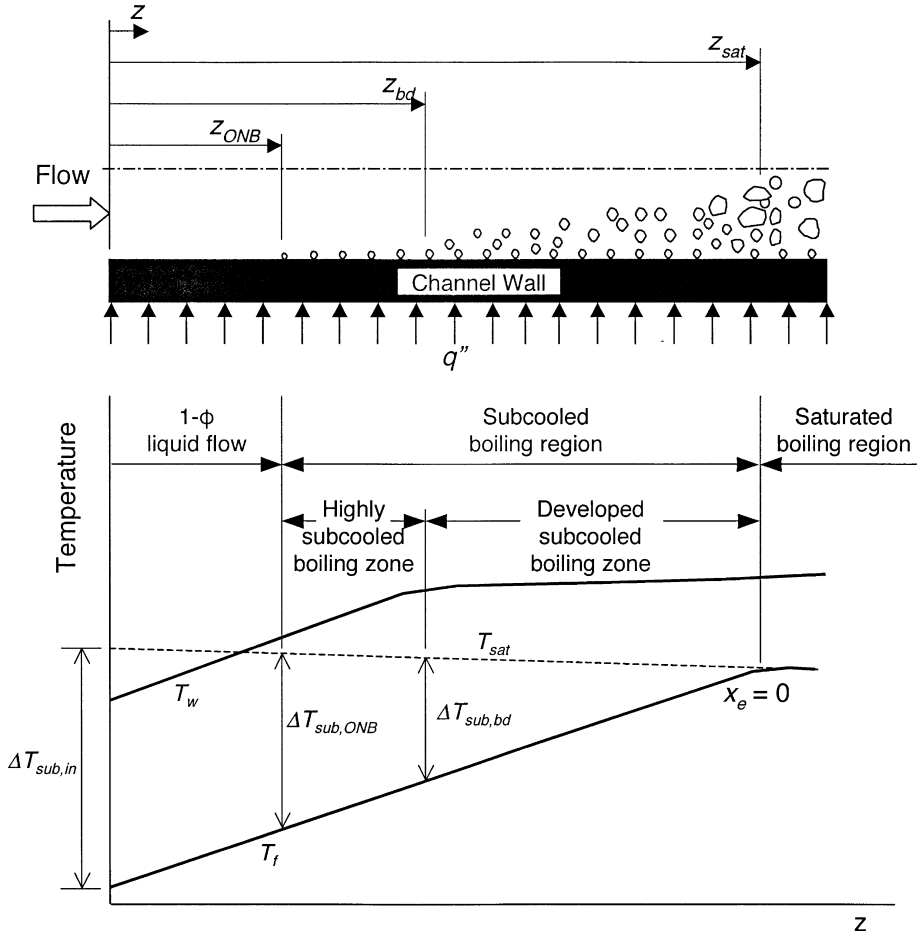

Fig. 1. Schematic representation of subcooled boiling zones.

to the location where thermodynamic equilibrium quality, defined as

$$x_e = \frac{h_f - h_{f,sat}}{h_{fg}}, \quad (1)$$

reaches zero. This location marks the upstream edge of the saturated boiling region. A key distinction between the highly subcooled zone and developed subcooled zone is that void fraction is a wall effect for the former and a bulk flow effect for the latter.

Existence of the two subcooled zones was verified in the flow visualization experiments discussed in part 1 of this study [1]. In these experiments, bubbles upstream of the departure point showed mild thermal growth while sliding along the wall. Downstream of the departure point, bubbles grew in size and were able to detach and coalesce with one another.

1.3. General trends of subcooled boiling pressure drop

As subcooled liquid heat ups along the wall of a heated channel, its viscosity decreases. Increasing the wall heat flux causes further reduction in liquid viscosity. Therefore, pressure drop associated with pure liquid flow decreases with increasing wall heat flux. The trend changes significantly when bubbles begins to form. Here, increasing wall heat flux increases both the two-phase frictional and accelerational gradients of pressure drop. Pressure drop therefore begins to increase with increasing heat flux. These trends are illustrated in Fig. 2 in the form of a normalized plot of pressure drop versus wall heat flux. The pressure drop, ΔP, for a given wall heat flux is normalized with respect to pressure drop corresponding to adiabatic flow, ΔP_{ad} ($q'' = 0$). Wall heat flux is normalized with respect to the value q''_{sat} of heat flux required to bring thermodynamic equilibrium quality of the flow to zero at the channel exit, where

$$q''_{sat} = \frac{\dot{m} c_{p,f} (T_{sat} - T_{in})}{A_{base}}. \quad (2)$$

Tong et al. [19] indicated the onset of nucleate boiling (ONB) does not coincide exactly with the point of minimum pressure drop in Fig. 2 and ONB generally occurs at a lower heat flux. One possible explanation for this offset is the existence of the highly subcooled zone. Because void fraction is quite small in this zone, any increases in two-phase frictional and accelerational pressure gradient are dwarfed by the pressure gradient of liquid, which covers a large fraction of wall area in the highly subcooled zone. The situation is quite different after the point of vapor departure, where the two-phase frictional and accelerational pressure gradients begin to increase substantially because of a large increase in void fraction.

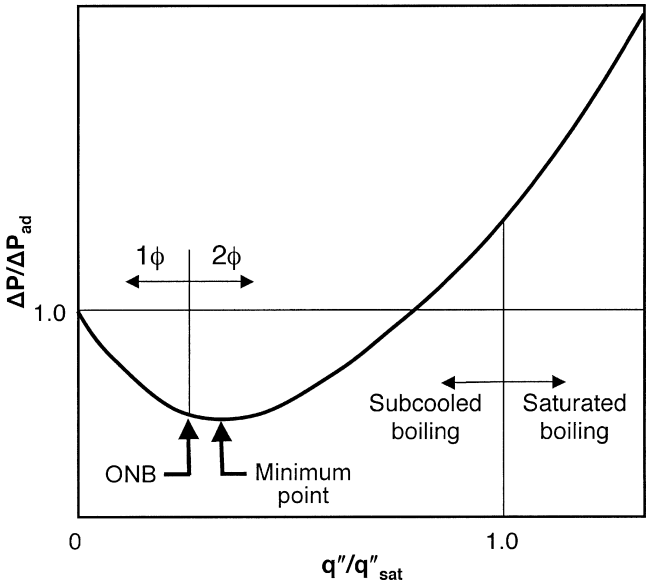

Fig. 2. Normalized plot of pressure drop versus wall heat flux for subcooled boiling.

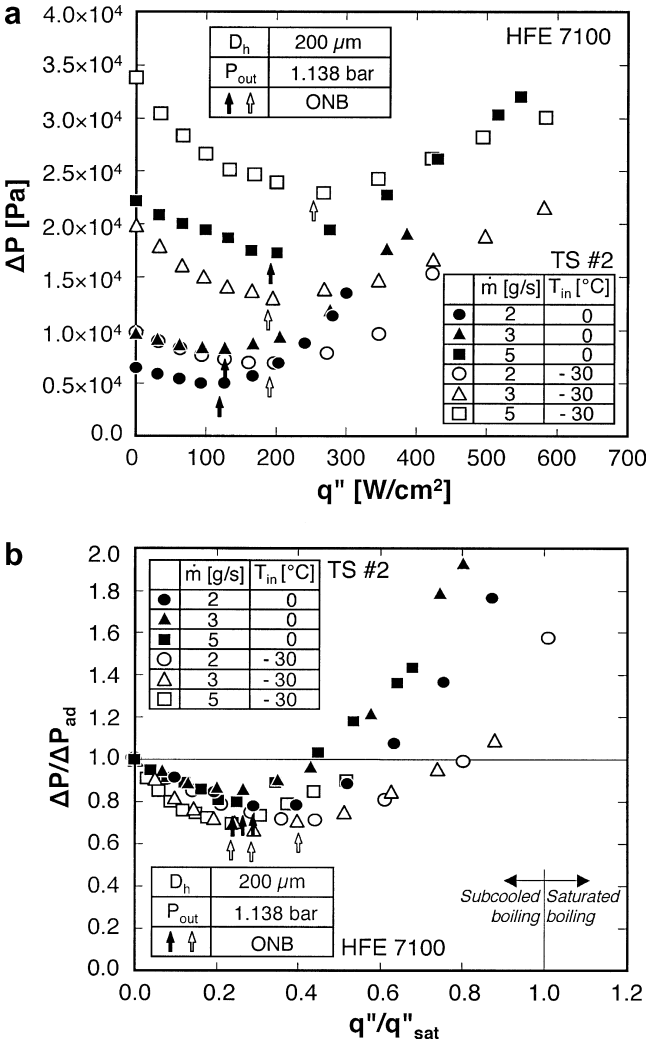

Fig. 3. (a) Variation of pressure drop for test section TS #2 ($D_h = 200$ μm) with heat flux for different flow rates and inlet temperatures, and (b) corresponding normalized pressure drop plot.

2. Pressure drop results

2.1. Experimental pressure drop results

Fig. 3 shows variations of measured pressure drop for test section TS #2 with heat flux for different flow rates and two inlet temperatures. Raw pressure drop data are presented in Fig. 3a and shown in normalized form in Fig. 3b. Details of the geometry and operating conditions for this and the other three tests sections are given in part 1 of this study [1]. Arrows in Fig. 3 indicate the observed ONB, which marks the onset of subcooled boiling. As suggested in the previous section, ONB occurs before the point of minimum pressure drop. In virtually all of the present data, an increase in the slope of pressure drop characteristics from the minimum point occurred with the first heat flux increment following ONB. This makes identifying any differences between ONB and point of vapor departure quite elusive. High heat fluxes and corresponding relatively large heat flux increments may have contributed to the difficulty capturing differences between the two conditions.

Fig. 3 also demonstrates a monotonic shift to higher pressure drop with increasing coolant flow rate as well as a corresponding delay in ONB to higher heat fluxes. However, the effect of subcooling is a bit more complex. As indicated in the previous section, pressure drop in the single-phase liquid region (before ONB) is highest for adiabatic flow and decreases with increasing heat flux due to decreasing liquid viscosity. Fig. 3a shows decreasing inlet liquid temperature causes a shift to higher pressure drop for a given flow rate because of increased liquid viscosity. However, decreasing the inlet temperature *decreases* the normalized pressure drop (see Fig. 3b) because of a stronger viscosity dependence on liquid temperature at lower temperatures. Fig. 3 also shows lower inlet temperatures delay ONB to higher heat fluxes, a trend that was captured in the flow visualization experiments discussed in part 1 of this study.

Fig. 3 shows the effect of decreasing inlet temperature is reversed in the subcooled boiling region. Here, lower inlet temperatures produce a relatively mild increase in pressure drop following ONB at −30 °C compared to 0 °C. This trend can be explained by the strong condensation effects at low inlet temperatures greatly reducing both void fraction and the overall influence of phase-change on pressure drop.

Fig. 4 shows the variation of pressure drop with heat flux for the four test sections. Indicated in this figure are mass velocity values for each test section corresponding to the same mass flow rate of 5 g/s. Pressure drop for the single-phase and two-phase regions can be represented, respectively, by

$$\left(\frac{dp}{dz}\right)_{sp,f} = \frac{2f_{sp}}{D_h} G^2 v_f \tag{3}$$

and

$$\left(\frac{dp}{dz}\right)_{tp} = \left(\frac{dp}{dz}\right)_{tp,F} + \left(\frac{dp}{dz}\right)_{tp,A} = \frac{2f_{tp}}{D_h} G^2 \bar{v} + G^2 \frac{d\bar{v}}{dz}, \tag{4}$$

where f_{sp} and f_{tp} are the single-phase and two-phase friction factors, respectively. Fig. 4 displays the strong depen-

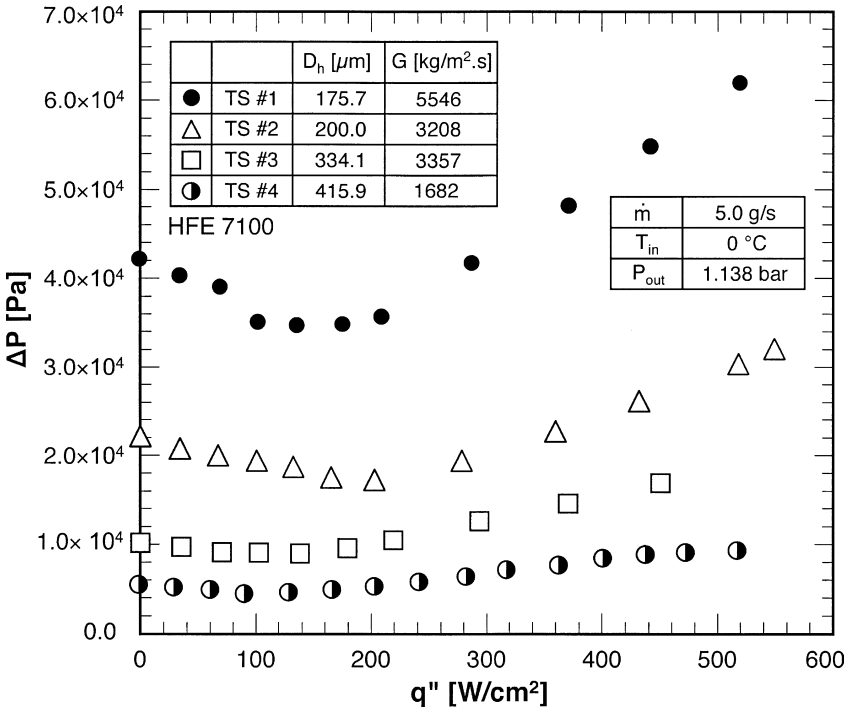

Fig. 4. Variation of pressure drop with heat flux for different micro-channel geometries and mass velocities.

dence of pressure drop on mass velocity evident in both of the above equations. Eqs. (3) and (4) also show pressure drop for both single-phase flow and two-phase flow increases with decreasing hydraulic diameter. This is also manifest in Fig. 4, where the highest pressure drop is associated with the smallest hydraulic diameter (TS #1, $D_h = 175.7$ μm) and largest mass velocity ($G = 5546$ kg/m^2 s).

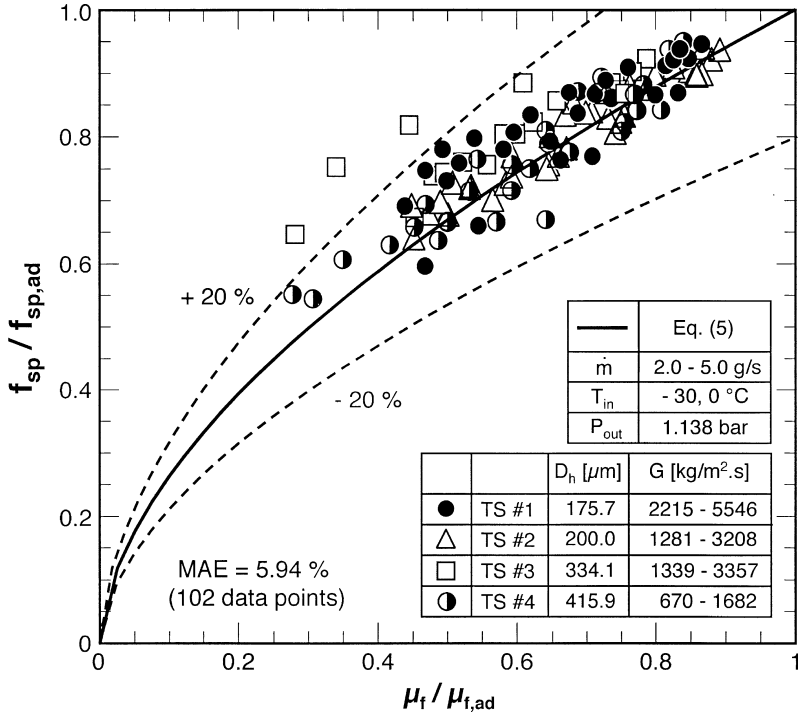

Fig. 5. Comparison of single-phase pressure drop data with predictions based on Eq. (5).

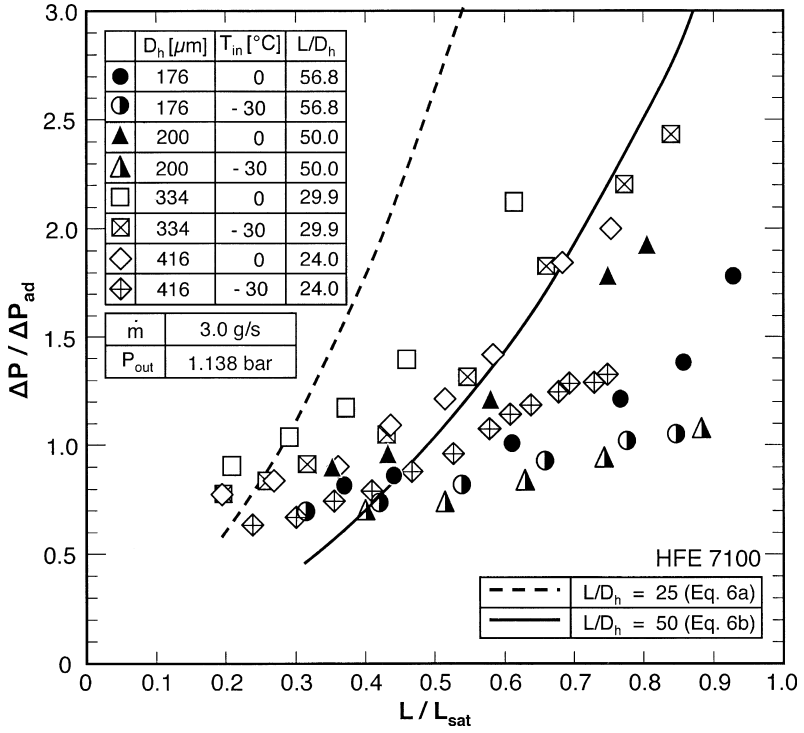

Fig. 6. Comparison of subcooled pressure drop data with predictions based on Eqs. (6a) and (6b).

2.2. Evaluation of prior correlations

Past studies have followed two general approaches to evaluating and correlating subcooled boiling pressure drop data. The first consists of evaluating the individual components of pressure drop, namely friction and acceleration (also gravity for inclined flows). An appropriate two-phase flow model is adopted in evaluating each component, and approximations are used to estimate friction factor as well as the relationship between quality and void fraction. In a recent publication [15], the authors of the present study summarized homogeneous and separated flow models for predicting pressure drop for two-phase micro-channel heat sinks. These models were intended for saturated flow boiling situations only.

One difficulty in utilizing this method here is the inability to determine the extent of the subcooled boiling region. Some authors suggested using the bubble departure point for this purpose (e.g., Bowring's analysis in [18] and [20]), but, as discussed earlier, there is no definitive assessment of the validity of this approach. Other difficulties stem from the inability to predict quality and void fraction in the subcooled region with a reasonable degree of certainty. Since thermodynamic equilibrium quality is negative in this region, an apparent non-equilibrium quality must be used instead. Hoffman et al. [21,22] examined available correlations for quality and void fraction to evaluate subcooled boiling pressure drop. Different correlations produced drastically different predictions and some yielded very unrealistic values.

The second approach to evaluating subcooled boiling pressure drop, which is adopted in the present study, is to normalize pressure drop data relative to adiabatic flow as discussed earlier in conjunction with Figs. 2 and 3. For the single-phase region, the present pressure drop data were compared to the following relation [23]:

$$\frac{\Delta P}{\Delta P_{ad}} = \frac{f_{sp}}{f_{sp,ad}} = \left(\frac{\mu_f}{\mu_{f,ad}}\right)^N, \tag{5}$$

where $N = 0.58$ for laminar heating. Fig. 5 shows Eq. (5) is quite successful at predicting pressure drop data for all four test sections corresponding to laminar flow with $Re_{Dh} < 1500$.

To determine ΔP using Eq. (5), the adiabatic pressure drop must first be determined by integrating Eq. (3) across the heat sink, taking into account the variation of friction factor along this predominantly developing flow. A detailed procedure for determining single-phase pressure drop for developing flow in rectangular micro-channels is provided in [12].

Bergles and Dormer [24] performed extensive subcooled boiling pressure drop measurements for a single tube diameter of 5.08 mm. They segregated their data according to pressure, subcooling and mass flux and developed chart type correlation plots for pressured drop estimation. Later, Tong et al. [19] combined their own data for $D_h = 1.05$–2.44 mm diameter tubes with the Bergles and Dormer charts and recommended replacing the earlier charts with the following correlation:

$$\frac{\Delta P}{\Delta P_{ad}} = \left(\frac{L_{sc}}{L_{sat}}\right)^{1.3} \exp\left\{\left(\frac{L_{sc}}{L_{sat}}\right) + 1.35\right\} \quad \text{for } L/D_h = 25 \tag{6a}$$

and

$$\frac{\Delta P}{\Delta P_{ad}} = \left(\frac{L_{sc}}{L_{sat}}\right)^{1.3} \exp\left\{\left(\frac{L_{sc}}{L_{sat}}\right) + 0.4\right\} \quad \text{for } L/D_h = 50, \tag{6b}$$

where L_{sc} and L_{sat} are, respectively, the length of the subcooled boiling region (from the end of the single-phase region) and the length measured from the inlet that is required to bring the fluid to saturated state. For a rectangular micro-channel, the latter length is given by

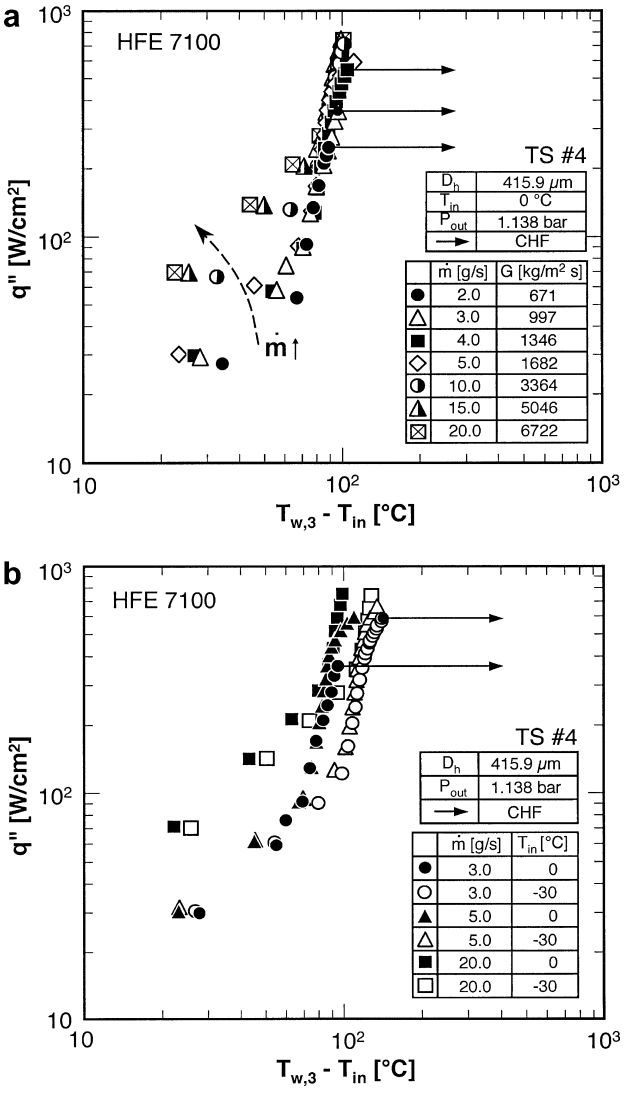

Fig. 7. Subcooled boiling curves for TS #4 ($D_h = 415.9$ μm) for (a) different flow rates and (b) different inlet temperatures.

$$L_{sat} = \frac{GW_{ch}H_{ch}}{q''(W_{ch}+W_w)} c_{p,f}(T_{sat} - T_{in}). \quad (7)$$

The L/D_h values for the test sections used in the present study are close to those given in Eqs. (6a) and (6b) ($L/D_h = 56.8$, 50.0, 29.9 and 24.0 for TS #1, TS #2, TS #3 and TS #4, respectively). However, estimating L_{sc} for the present data is quite difficult because of both the small length of the micro-channels and the difficulty detecting ONB. To resolve this problem, only data corresponding to conditions where subcooled boiling was observed over the entire length (i.e., $L_{sc} = L$) are examined. Fig. 6 shows significant departure of predictions based on Eqs. (6a) and (6b) from those specific data in terms of both slope and magnitude. This departure can be attributed to several factors. First, the two correlations contain five key parameters: mass velocity, inlet subcooling, outlet pressure, and two geometrical parameters (D_h and L/D_h ratio). There are appreciable differences between the parameters of the database from which the correlations were derived and those of the present study. For example, hydraulic diameter is 2.5–14 times smaller, mass velocity 5–60 times smaller, and pressure 6–9 times lower than the earlier database. Another key difference is working fluid. Past correlations, which were intended mainly for nuclear applications, used water as working fluid. The fluid used in the present study, HFE 7100, has far smaller latent heat of vaporization and surface tension than water; it is also far more wetting.

The weak predictions displayed in Fig. 6 highlight the need for new models and/or correlations that are specifically suited for micro-channel flows and which can tackle different types of fluids. Those are key objectives of ongoing research efforts by the authors.

3. Heat transfer results

3.1. Boiling curves

Fig. 7 shows boiling curves for TS #4, which has the largest hydraulic diameter of $D_h = 416$ μm. These tests produced remarkable performance, exceeding 700 W/cm^2 for the highest mass velocity case. Interestingly, the relatively large hydraulic diameter for this particular test section produced the lowest mass velocity for a given flow rate compared to the other three test sections. This resulted in poorer cooling performance for TS #4 than the other test sections. This implies cooling performance well above 700 W/cm^2 is possible with the smaller hydraulic diameters. Those cases were not attempted because their pressure drop at high mass velocities exceeded the capability of the pump used in the present study. Efforts are underway to modify the loop in preparation for future experiments involving high flow rates with the three smaller hydraulic diameters.

Fig. 7a shows the effects of mass flow rate on boiling performance for TS #4. With the inlet temperature held constant, there is very little effect of flow rate on the nucleate boiling region. This means the heat transfer coefficient in this region is independent of mass velocity. The effects of flow rate are evident mostly in the single-phase region and at CHF. Higher flow rates are shown shifting the single-phase data upwards and delaying ONB to higher heat fluxes and higher surface temperatures. Higher CHF values are also achieved by increasing the flow rate. Notice that CHF conditions were reached with only the lower flow rates. Since the nucleate boiling region for the higher flow

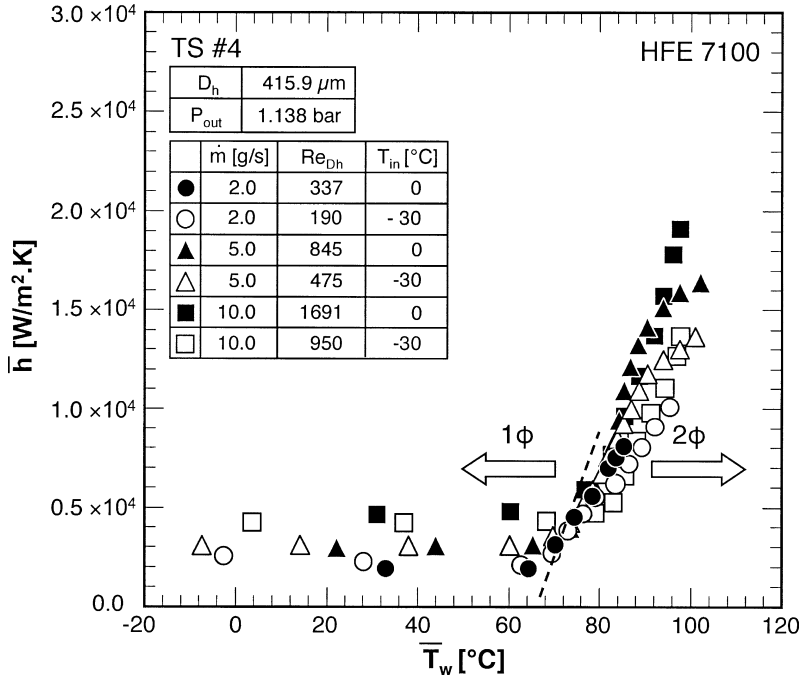

Fig. 8. Variation of mean heat transfer coefficient with mean wall temperature for test section TS #4 for different flow rates and two inlet temperatures.

rates exceeded 700 W/cm^2, temperatures in the test module were quite elevated for both the cartridge heaters and fiberglass plastic parts, prompting the operator to halt the testing even before CHF was reached. Efforts are underway to improve the test module's design to enable future testing at yet higher heat fluxes.

Fig. 7b shows the effects of inlet temperature on boiling performance. Prominently captured in this plot are the two distinct nucleate boiling regions, each is associated with a different inlet temperature. This departure is the result of representing the temperature axis as the difference between wall and inlet rather than saturation temperature. Increasing subcooling is shown delaying ONB and increasing CHF.

3.2. Heat transfer coefficient data

Fig. 8 shows for TS #4 the variation of mean heat transfer coefficient, which is average of local heat transfer coefficients for three micro-channel base locations above the thermocouples, with the mean of the three base temperatures at the same locations. Values of the local heat transfer coefficient and channel bottom wall temperature were determined using an iterative technique described in part 1 of this study [1]. With a saturation temperature for HFE 7100 of 63 °C (based on outlet pressure), Fig. 8 shows phase-change occurs 5–14 °C above saturation temperature, depending on flow rate and inlet temperature. Before this point, cooling is the result of single-phase heat transfer

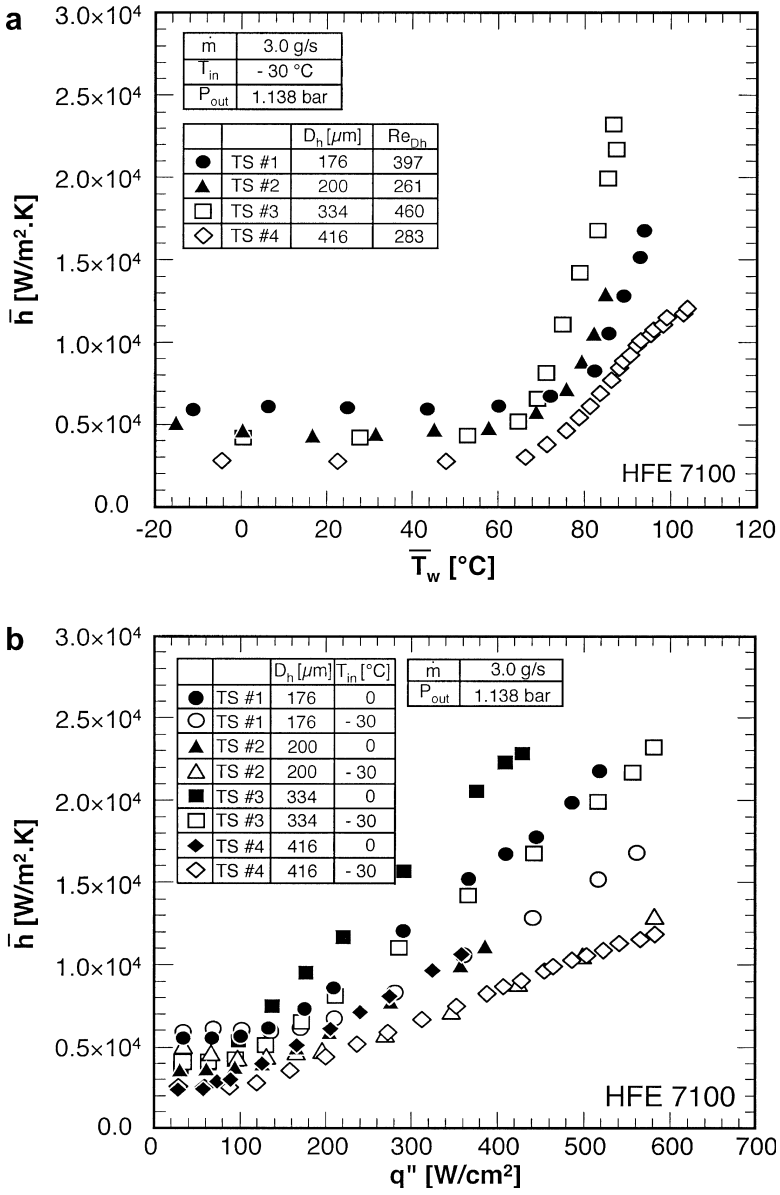

Fig. 9. (a) Variation of average heat transfer coefficient with average wall temperature for different hydraulic diameters. (b) Variation of average heat transfer coefficient with heat flux for different hydraulic diameters and two inlet temperatures.

to liquid. The transition to nucleate boiling is marked by a sharp increase in the magnitude of the heat transfer coefficient.

For fully developed laminar internal flow, single-phase heat transfer is associated with a constant Nusselt number, regardless of mass flow rate. However, Fig. 8 shows mild changes in the heat transfer coefficient with flow rate because most of the micro-channel length in the present study consisted of developing entrance flow. Within this region, increasing mass flow rate (and therefore Reynolds number) increases the extent of the entrance region, resulting in a higher average single-phase heat transfer coefficient. Inlet temperature has a relatively minor effect, mostly in the form of mild variations in liquid properties. Fig. 8 shows nucleate boiling data follow a well-defined trend, fairly independent of flow rate or inlet subcooling except for near-CHF data.

Fig. 9a shows the variation of average heat transfer coefficient with mean wall temperature for the four test sections at the same inlet temperature and same flow rate. For fully developed laminar flow, the heat transfer coefficient is inversely proportional to hydraulic diameter. However, as discussed above, heat transfer coefficient in the present study is strongly influenced by entrance effects. Fig. 9a shows TS #1, which has the smallest hydraulic diameter of $D_h = 176$ μm, yields the highest single-phase heat transfer coefficient. However, TS #2 (200 μm) and TS #3 (334 μm) yield fairly equal $\bar{h}$ values despite the large difference in their hydraulic diameters. This trend can be explained by the increased $\bar{h}$ for TS #3 resulting from a higher Reynolds number. There are also secondary effects for all tests sections resulting from micro-channel aspect ratio.

The nucleate boiling data in Fig. 9a shows a more complicated trend. Here, TS #4, which has the largest hydraulic diameter and therefore smallest mass velocity, shows the poorest two-phase performance. However, the highest heat transfer coefficients are achieved with TS #3 followed by TS #2 and then TS #1. Therefore, decreasing hydraulic diameter does not yield a monotonic increase in two-phase heat transfer coefficient. Secondary effects, such as channel width, sidewall thickness and aspect ratio, must play additional role.

This complex trend may be explained by the flow visualization results discussed in part 1 of this study. Aside from its larger D_h and lower G compared to both TS #1 and TS #2, TS #3 also has larger micro-channel width, W_{ch}. As discussed in part 1, narrow width facilitates earlier transition from bubbly to slug flow, which suppresses nucleate boiling activity and reduces the two-phase heat transfer coefficient. This is clearly manifested in Fig. 9a in the form of superior two-phase performance for TS #3 compared to both TS #1 and TS #2. This may also be the reason why TS #2 provides better two-phase heat transfer performance compared to TS #1. While both have the same micro-channel width and wall thickness, TS #2 has deeper micro-channels (i.e., larger H_{ch}), allowing more room for bubbles to move along the micro-channel with reduced interaction with other bubbles compared to TS #1.

The effects of hydraulic diameter and subcooling on the two-phase heat transfer coefficient are also shown in Fig. 9b. For a given heat flux, smaller micro-channels delay the commencement of subcooled boiling because of both their high mass velocity and increased wetted area, as discussed in part I. Higher subcooling produces a similar trend.

3.3. Evaluation of prior correlations

Very few correlations are available in the literature for the prediction of subcooled boiling heat transfer. Table 1

Table 1
Subcooled boiling heat transfer correlations

Author(s)	Correlations		MAE	Remarks
Shah [25]	$q'' = 230Bo^{0.5}h_{sp}\Delta T_{sat}, \quad Bo = \frac{q''}{Gh_{fg}}$	(8)	35.1%	Saturated boiling (various Newtonian fluids except liquid metals)
Shah [26]	$q'' = 0.54\{230Bo^{0.5}h_{sp}\}(\Delta T_{sub})^{7.83/8.33}(\Delta T_{sat})^{1/8.33}$, where $\Delta T_{sat} = T_w - T_{sat}$ and $\Delta T_{sub} = T_{sat} - T_f$	(9)	44.3%	Subcooled boiling (water, ammonia, refrigerants, alcohols, CCl_4, K_2CO_3, etc.)
Kandlikar [28]	$q'' = [1058(Gh_{fg})^{-0.7}F_f h_{sp}\Delta T_{sat}]^{1/0.3}, \quad F_f = 1.0$ for water	(10)	313%	Water subcooled boiling
	$q'' = [1058(Gh_{fg})^{-0.7}F_f h_{sp}\Delta T_{sat}]^{1/0.3}, \quad F_f = 1.5$ for R-12	(11)	1381%	Refrigerant subcooled boiling (other F_f values recommended for different refrigerants)
Papell [29]	$\frac{Nu_{tp}}{Nu_{sp}} = 90.0Bo^{0.7}\left(\frac{h_{fg}}{c_{p,f}\Delta T_{sub}}\right)^{0.84}\left(\frac{\rho_g}{\rho_f}\right)^{0.756}$	(12)	69.8%	Water, ammonia
Moles and Shaw [30]	$\frac{Nu_{tp}}{Nu_{sp}} = 78.5Bo^{0.67}\left(\frac{h_{fg}}{c_{p,f}\Delta T_{sub}}\right)^{0.50}\left(\frac{\rho_g}{\rho_f}\right)^{-0.03}Pr_f^{0.45}$	(13)	658%	Water, acetone, isopropyl alcohol

provides a select summary of correlations whose predictions are compared to the present data. The Shah correlation for saturated boiling has shown favorable predictive capability for macro circular tubes [25]. He later modified his original correlation to tackle subcooled boiling as well [26]. Kandlikar also developed a correlation for saturated boiling [27], which he later modified to fit subcooled boiling data for two types of fluids, water and refrigerant R-12 [28]. The correlations of both Shah and Kandlikar require knowledge of the single-phase heat transfer coefficient, h_{sp}. Since the primary goal here is to assess the capability of correlations at predicting the two-phase heat transfer, h_{sp} in these correlations was replaced by mean values measured in the present study.

Fig. 10 compares predictions based on the Shah saturated and subcooled boiling correlations, as well as Kandlikar's subcooled boiling correlations, to present data for the four tests sections corresponding to $T_{in} = 0$ °C. Kandlikar's saturated boiling correlation is excluded because it yielded unusually poor predictions. In the initial stages of the subcooled boiling region, Fig. 10 shows Shah's subcooled boiling correlation overpredicts the present data, while his saturated boiling correlation underpredicts; the data fall midway between the two. However, Shah's two correlations and the present data do converge at the end of the subcooled boiling region. Kandlikar correlations on the other hand show poor overall predictions. Fig. 11 shows fairly similar predictive trends for $T_{in} = -30$ °C.

Another type of subcooled boiling correlation consists of presenting the ratio of subcooled boiling Nusselt number to single-phase Nusselt number as a function of boiling number, Jacob number, and density ratio. Such are the correlations by Papell [29] and Moles and Shaw [30]. Fig. 12 shows the Papell correlation predicts the present data with a mean absolute error of 69.8%. Interestingly, better predictions are achieved with lower aspect ratio test sections

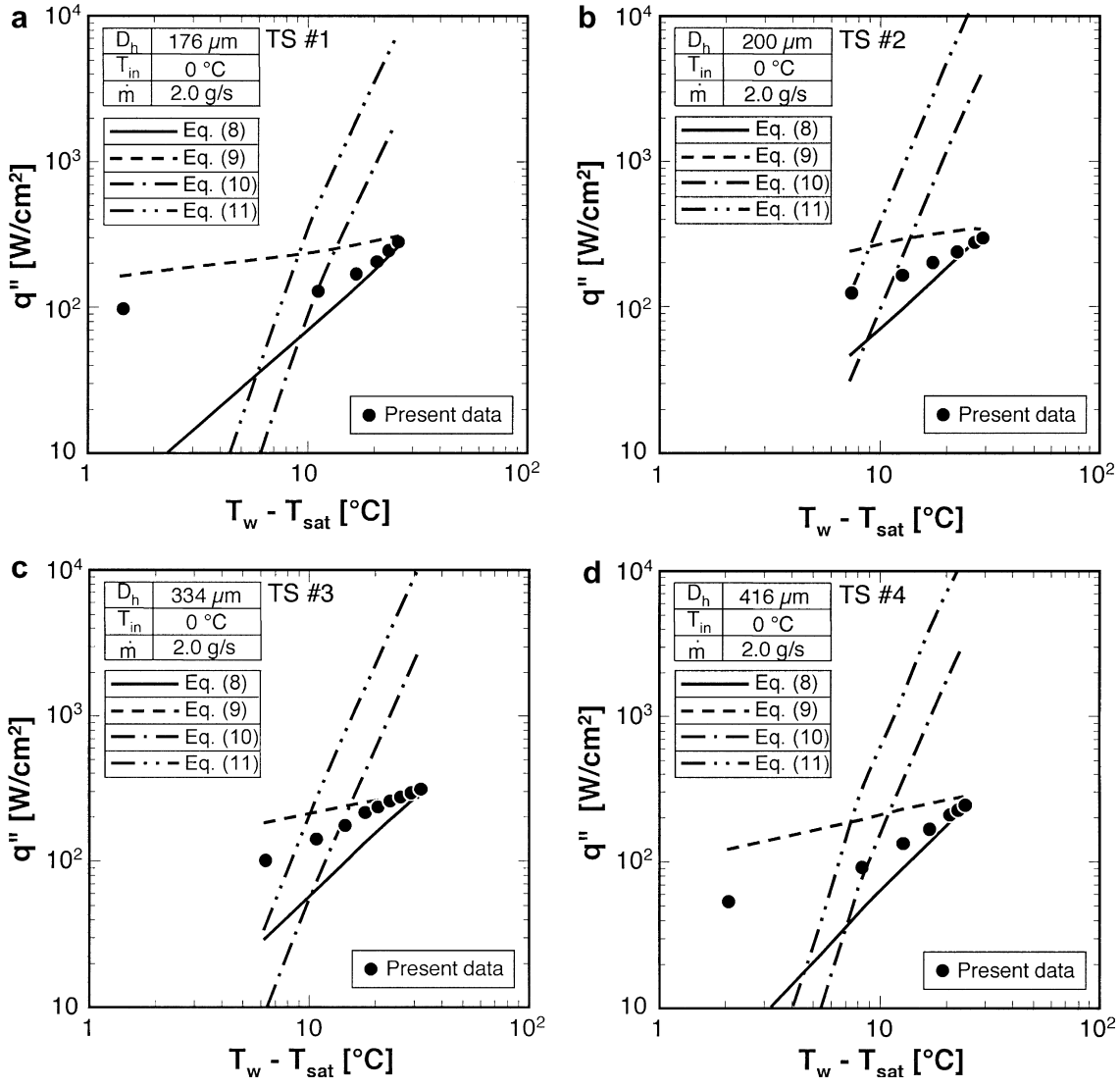

Fig. 10. Comparison of predictions of prior two-phase heat transfer correlations and present subcooled boiling data corresponding to $T_{in} = 0$ °C for (a) TS #1, (b) TS #2, (c) TS #3, and (d) TS #4.

(TS #1 and TS #3) than those with higher aspect ratio (TS #2 and TS #4). However, it is difficult to draw definitive conclusions about this trend in the absence of any geometrical parameters in the correlation itself. Table 1 shows predictions of the Moles and Shaw correlation are far worse than those of Papell's.

3.4. New correlations

While none of the prior correlations provided accurate predictions, Shah's saturated and subcooled correlations showed some promise. Since the present data fell about halfway between the two correlations, the following new correlation was derived that yields values close to the mean of these correlations

$$q'' = 230Bo^{0.5}h_{sp}[0.828\Delta T_{sat} + 0.463\Delta T_{sat}^{-0.04}\Delta T_{sub}^{0.81}]. \quad (14)$$

In this equation, the boiling number dependence of the original correlations was preserved, but the dependence on wall superheat and subcooling was adjusted to yield least mean absolute error from the data. Fig. 13 shows this new correlation predicts 260 heat transfer data points for all four test sections with a mean absolute error of 9.1%, with almost all the data falling within ±30% of predicted values.

A key drawback in using Eq. (14) is the difficulty directly inferring the magnitude of the heat transfer coefficient. A second correlation is therefore suggested for direct estimation of the subcooled boiling heat transfer coefficient. Like the second group of correlations in Table 1, the normalized two-phase Nusselt number is correlated according to the form

$$\frac{Nu_{tp}}{Nu_{sp}} = 90.0Bo^{0.9}Ja^{*-0.98}We^{*0.15}\beta^{-0.42}, \quad (15)$$

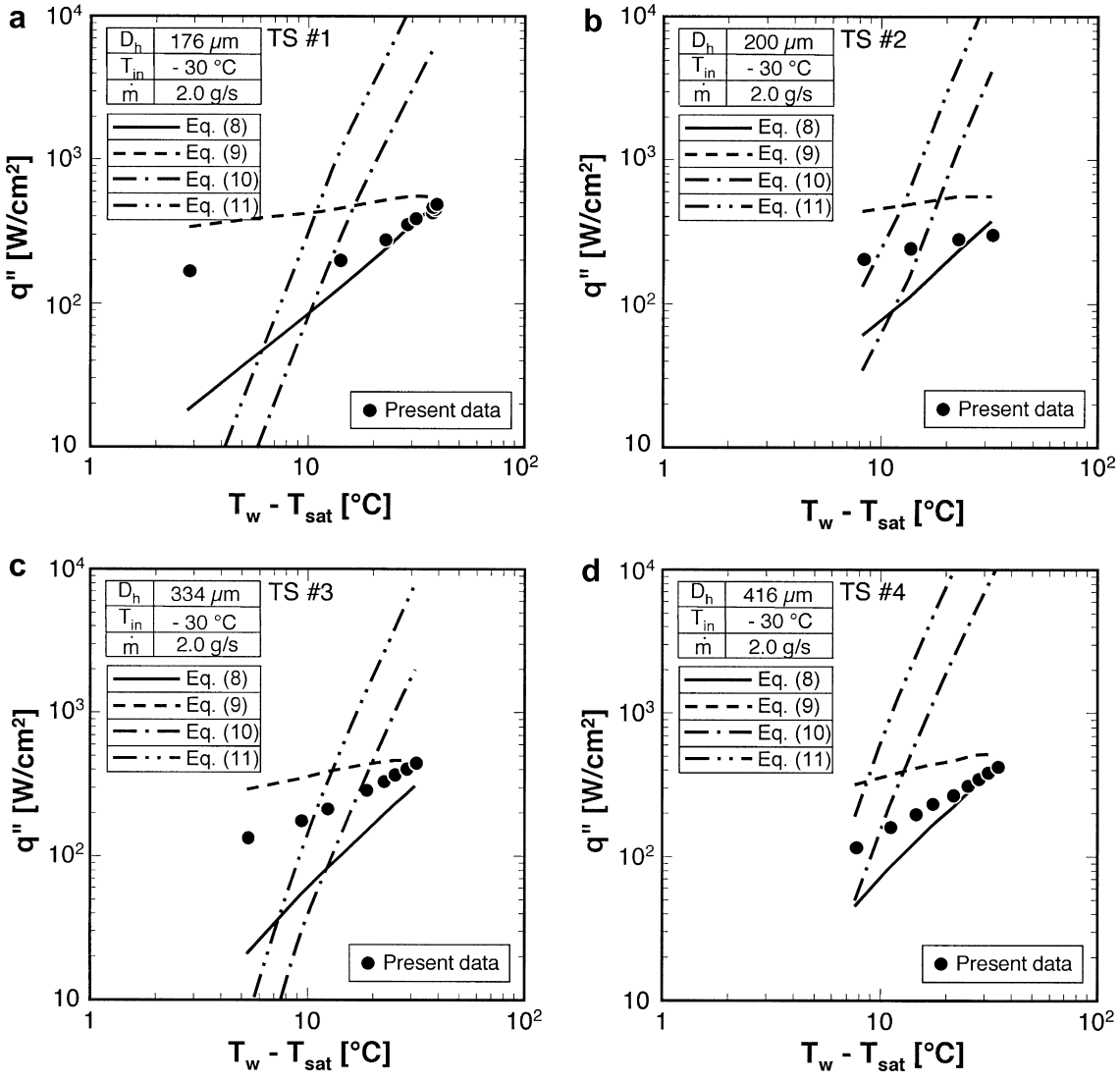

Fig. 11. Comparison of predictions of prior two-phase heat transfer correlations and present subcooled boiling data corresponding to $T_{in} = -30$ °C for (a) TS #1, (b) TS #2, (c) TS #3, and (d) TS #4.

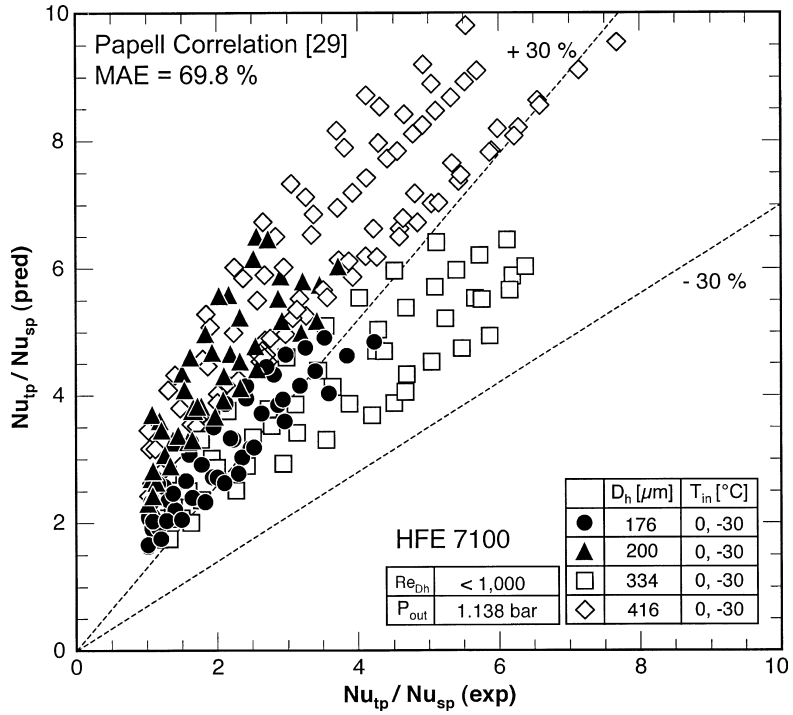

Fig. 12. Comparison of predictions of Papell's correlation and present subcooled boiling data.

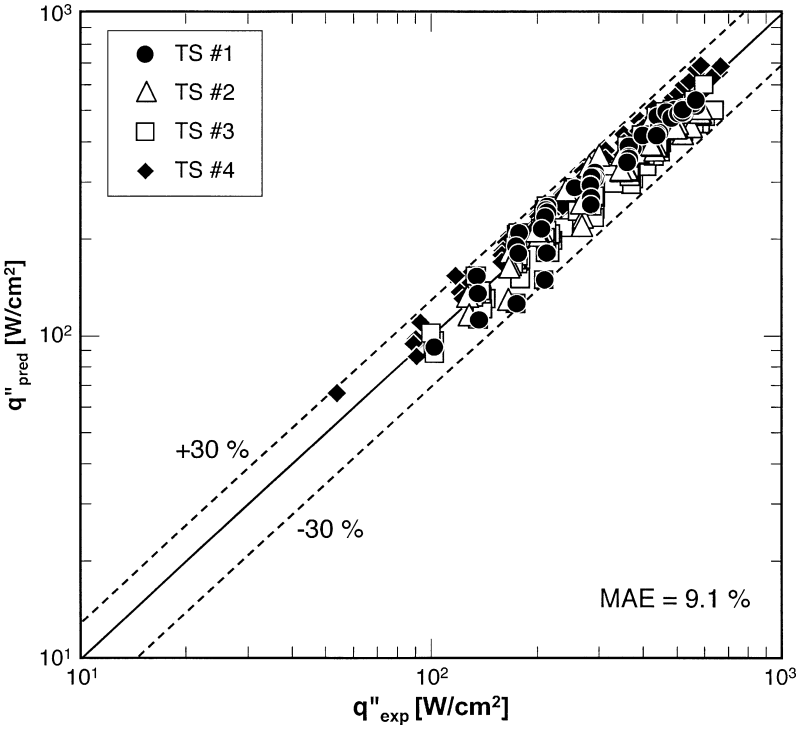

Fig. 13. Comparison of predictions of new modified Shah correlation and subcooled boiling data for four test sections.

where

$$Ja^* = \frac{c_{p,f}\Delta T_{sub,in}}{h_{fg}}, \quad We^* = \frac{G^2 D_h}{(\rho_f - \rho_g)\sigma}, \quad \text{and} \quad \beta = \frac{H_{ch}}{W_{ch}}. \tag{16}$$

Unlike earlier correlations, Eq. (15) accounts for all relevant physical parameters of subcooled flow boiling in micro-channels. The effects of heat flux, inlet subcooling, surface tension and geometry are accounted for in four respective dimensionless groups: boiling number, Jacob

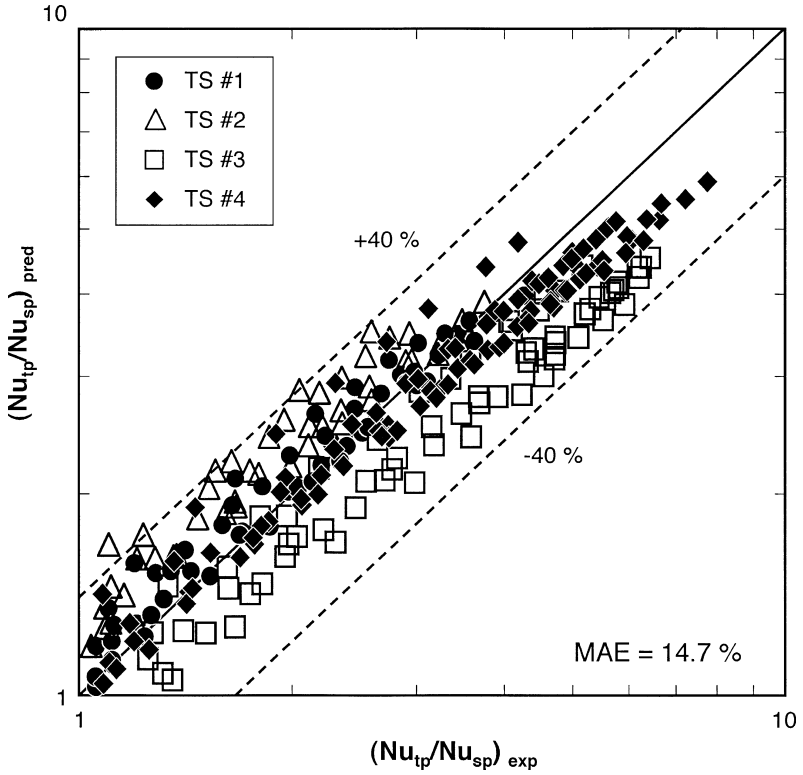

Fig. 14. Comparison of predictions of new normalized two-phase Nusselt number correlation and experimental data for four test sections.

number, Weber number and channel aspect ratio. Fig. 14 compares the predictions of this new correlation with experimental data for the four test sections. Although the mean absolute error for this correlation is greater than for Eqs. (14, 15), enables direct calculation of the two-phase heat transfer coefficient as well as accounts for all the parameters that were shown in part 1 of this study to influence cooling performance.

4. Conclusions

Experiments were performed to determine both the pressure drop and heat transfer characteristics of two-phase micro-channel flow. Unlike earlier studies of two-phase heat sinks, where annular evaporation is typically the dominant mechanism for heat removal, the present work focused on subcooled boiling characteristics. Four different test sections were tested to assess the effects of not only hydraulic diameter, but micro-channel width and aspect ratio as well. Aided by findings from the flow visualization study presented in part 1, the data were carefully examined for important parametric trends and compared to predictions of earlier correlations. Key findings from this study are as follows.

(1) During single-phase cooling, pressure drop decreases with increasing heat flux because of decreased liquid viscosity. After bubbles form and depart into the liquid flow, void fraction begins to increase appreciably, causing pressure drop to begin increasing with increasing heat flux. These opposite trends produce a minimum in the variation of pressure drop with heat flux.
(2) Increasing the subcooling of incoming liquid decreases two-phase pressure drop because of decreased void fraction caused by strong condensation at bubble interfaces, and decreased likelihood of bubble coalescence.
(3) The effects of hydraulic diameter on two-phase heat transfer are complicated by the relative size of bubbles and micro-channel width. While smaller hydraulic diameters tend to enhance two-phase cooling performance by increasing both mass velocity and wetted area, smaller micro-channel width can trigger early transition from bubbly to slug flow, causing a reduction in cooling effectiveness.
(4) It is quite difficult to identify correlations from the heat transfer literature that can predict pressure drop and cooling behavior of subcooled micro-channel heat sinks. This difficulty is the result of scarcity of subcooled boiling correlations in general, and the drastic differences in fluid, hydraulic diameter, and operating conditions of the present study compared to the macro-channel heat transfer databases upon which these correlations are based. Two new modified forms of earlier correlations produced good predictions of the present heat transfer data.
(5) The shortage of useful correlations highlights the need for new mechanistic models of subcooled micro-channel boiling that capture the complex inter-

facial interactions reported in part 1 of this study. Such models are the goals of ongoing studies by the authors.

Acknowledgement

The authors are grateful for the support of the Office of Naval Research (ONR) for this study.

References

[1] J. Lee, I. Mudawar, Fluid flow and heat transfer characteristics of low temperature two-phase micro-channel heat sinks – Part 1. Experimental methods and flow visualization results, Int. J. Heat Mass Transfer, in press, doi:10.1016/j.ijheatmasstransfer.2008.02.012.
[2] D.B. Tuckerman, R.F.W. Pease, High-performance heat sinking for VLSI, IEEE Electron. Devices Lett. 2 (1981) 126–129.
[3] I. Mudawar, M.A. El-Masri, C.S. Wu, J.R. Ausman-Mudawar, Boiling heat transfer and critical heat flux in high-speed rotating liquid films, Int. J. Heat Mass Transfer 28 (1985) 795–806.
[4] M.B. Bowers, I. Mudawar, High flux boiling in low flow rate, low pressure drop mini-channel and micro-channel heat sinks, Int. J. Heat Mass Transfer 37 (1994) 321–332.
[5] M.B. Bowers, I. Mudawar, Two-phase electronic cooling using mini-channel and micro-channel heat sinks: Part 1 – Design criteria and heat diffusion constraints, ASME J. Electron. Packaging 116 (1994) 290–297.
[6] M.B. Bowers, I. Mudawar, Two-phase electronic cooling using mini-channel and micro-channel heat sinks: Part 2 – Flow rate and pressure drop constraints, ASME J. Electron. Packaging 116 (1994) 298–305.
[7] I. Mudawar, M.B. Bowers, Ultra-high critical heat flux (CHF) for subcooled water flow boiling – I. CHF data and parametric effects for small diameter tubes, Int. J. Heat Mass Transfer 42 (1999) 1405–1428.
[8] H.J. Lee, S.Y. Lee, Heat transfer correlation for boiling flows in small rectangular horizontal channels with low aspect ratios, Int. J. Multiphase Flow 27 (2001) 2043–2062.
[9] H.J. Lee, S.Y. Lee, Pressure drop correlations for two-phase flow within horizontal rectangular channels with small heights, Int. J. Multiphase Flow 27 (2001) 783–796.
[10] W. Yu, D.M. France, M.W. Wambsganss, J.R. Hull, Two-phase pressure drop, boiling heat transfer, and critical heat flux to water in a small-diameter horizontal tube, Int. J. Multiphase Flow 28 (2002) 927–941.
[11] W. Qu, I. Mudawar, Prediction and measurement of incipient boiling heat flux in micro-channel heat sinks, Int. J. Heat Mass Transfer 45 (2002) 3933–3945.
[12] W. Qu, I. Mudawar, Measurement and prediction of pressure drop in two-phase micro-channel heat sinks, Int. J. Heat Mass Transfer 46 (2003) 2737–2753.
[13] W. Qu, I. Mudawar, Flow boiling heat transfer in two-phase micro-channel heat sinks – I. Experimental investigation and assessment of correlation methods, Int. J. Heat Mass Transfer 46 (2003) 2755–2771.
[14] W. Qu, I. Mudawar, Flow boiling heat transfer in two-phase micro-channel heat sinks – II. Annular two-phase flow model, Int. J. Heat Mass Transfer 46 (2003) 2773–2784.
[15] J. Lee, I. Mudawar, Two-phase flow in high-heat-flux micro-channel heat sink for refrigeration cooling applications: Part I. Pressure drop characteristics, Int. J. Heat Mass Transfer 48 (2005) 928–940.
[16] J. Lee, I. Mudawar, Two-phase flow in high-heat-flux micro-channel heat sink for refrigeration cooling applications: Part II. Heat transfer characteristics, Int. J. Heat Mass Transfer 48 (2005) 941–955.
[17] I. Mudawar, Assessment of high-heat-flux thermal management schemes, IEEE Trans. – CPMT: Components and Packaging Technologies 24 (2001) 122–141.
[18] J.G. Collier, J.R. Thome, Convective Boiling and Condensation, 3rd ed., Oxford University Press, New York, 1994, pp. 183–213.
[19] W. Tong, A.E. Bergles, M.K. Jensen, Pressure drop with highly subcooled flow boiling in small-diameter tubes, Exp. Therm. Fluid Sci. 15 (1997) 202–212.
[20] P. Saha, N. Zuber, Point of net vapor generation and vapor void fraction in subcooled boiling, in: Heat Transfer 1974, vol. 4, Proceedings of the 5th International Heat Transfer Conference, Tokyo, 1974, pp. 175–179.
[21] M.A. Hoffman, C.T. Kline, Evaluation of several empirical models for predicting subcooled flow-boiling pressure drop, in: V.K. Dhir, J.C. Chen, O.C. Jones (Eds.), Multiphase Flow and Heat Transfer, 23rd National Heat Transfer Conference, ASME HTD, vol. 47, Denver, CO, 1985, pp. 151–160.
[22] M.A. Hoffman, C.F. Wong, Prediction of pressure drops in forced convection subcooled boiling water flows, Int. J. Heat Mass Transfer 35 (1992) 3291–3299.
[23] W.K. Kays, M.E. Crawford, Convective Heat and Mass Transfer, 2nd ed., McGraw-Hill, New York, 1980, pp. 275–280.
[24] A.E. Bergles, T. Dormer Jr., Subcooled boiling pressure drop with water at low pressure, Int. J. Heat Mass Transfer 12 (1969) 459–470.
[25] M.M. Shah, A new correlation for heat transfer during boiling flow through pipes, ASHRAE Trans. 82 (1976) 66–86.
[26] M.M. Shah, A general correlation for heat transfer during subcooled boiling in pipes and annuli, ASHRAE Trans. 83 (1977) 202–217.
[27] S.G. Kandlikar, A general correlation for saturated two-phase flow boiling heat transfer inside horizontal and vertical tubes, ASME J. Heat Transfer 112 (1990) 219–228.
[28] S.G. Kandlikar, Heat transfer characteristics in partial boiling, fully developed boiling, and significant void flow regions of subcooled flow boiling, ASME J. Heat Transfer 120 (1998) 395–401.
[29] S.S. Papell, Subcooled boiling heat transfer under forced convection in a heated tube, NASA Technical Note D-1583, Lewis Research Center, Cleveland, OH, 1963.
[30] F.D. Moles, J.F.G. Shaw, Boiling heat transfer to subcooled liquids under condition of forced convection, Trans. Inst. Chem. Eng. 50 (1972) 76–84.